UNIVERSITÀ DEGLI STUDI DI TRENTO

This is an author's version of the contribution published on:

C-C. Chou, E. Lepore, P. Antonaci, N.M. Pugno, M.J. Buehler. Mechanics of trichocyte alpha-keratin fibers: Experiment, theory, and simulation. *Journal of Materials Research*. 30(1):26-35, 2015. [http://dx.doi.org/10.1557/jmr.2014.267]

The final version is available at the following URL:

http://journals.cambridge.org/action/displayAbstract?fromPage=online&aid=9520394&fileId=S0884291414002672

Mechanics of trichocyte alpha-keratin fibers: Experiment, theory and simulation

Chia-Ching Chou[1], Emiliano Lepore[2], Paola Antonaci[3], Nicola Pugno[2,4,5,*] and Markus J. Buehler[1*]

[1] *Laboratory for Atomistic and Molecular Mechanics, Department of Civil and Environmental Engineering, Massachusetts Institute of Technology, 77 Mass. Ave. Room 1-235A&B, Cambridge, MA, 02139, USA*
[2]*Laboratory of Bio-inspired & Graphene Nanomechanics, Department of Civil, Environmental and Mechanical Engineering, University of Trento, via Mesiano, 77, 38123 Trento, Italy*
[3]*Laboratory of Bio-Inspired Nanomechanics "Giuseppe Maria Pugno", Department of Structural Engineering and Geotechnics, Politecnico di Torino, Corso Duca degli Abruzzi 24, 10129 Torino, Italy*
[4]*Center for Materials & Microsystems, Fondazione Bruno Kessler, via Sommarive 18, 38123 Povo (Trento), Italy*
[5]*School of Engineering & Materials Science, Queen Mary University of London, Mile End Road, London E1 4NS, UK*

** Corresponding authors, E-mail: nicola.pugno@unitn.it & mbuehler@MIT.EDU*

ABSTRACT: The mechanical behavior of human hair is determined by interaction of trichocyte alpha keratin protein, matrix and disulfide bonds crosslinking between alpha-keratin and matrix. Much effort has been spent to understand the link between the microscopic structure and the macroscopic fiber properties. Here we apply a mesoscopic coarse-grained model of the keratin macrofilament fibril and an analytical solution based on the concept of entropic hyperelasticity of the protein helix to investigate the link between the microscopic structure and the macroscopic properties of keratin fibres.
The mesoscopic model provides good agreement with a wide range of experimental results. Based on the mesoscopic model, the predicted stress-strain curve of hair fibers agrees well with our own experimental measurements. The disulfide crosslink the microfibril-matrix and matrix-matrix contributes to the initial modulus and provides stiffening at larger deformation of trichocyte keratin fibers. The results show that the disulfide bonds reinforce the macrofilament and enhance the robustness of the macrofilament by facilitating the microfilaments to deform cooperatively. The availability of a mesoscopic model of this protein opens the possibility to further explore the relationship between microscopic chemical structure and macroscopic performance for a bottom-up description of soft materials.

Keywords: Keratin; Hair; Mesoscale model; Disulfide bond; Alpha helix protein

Submitted to: *Journal of Materials Research (Focus Issue: Soft Nanomaterials)*

Introduction

Hair fiber is a hierarchical structure ranging from alpha-helix, coiled-coils, microfibrils, macrofibrils to fibers, as sketched in **Figure 1(A)**. The primary structural molecules in wool and hair fibers are keratin intermediate filament (IF) proteins, forming a microfibril which is built from the assembly of coiled-coils (heterodimers). The IF is embedded in a sulfur-rich protein matrix and assembles into macrofibrils. For keratinized materials, the elastic modulus ranges from approximately 1-4 GPa. For example, the modulus is 1.6-4.5 GPa[1,2] in wool, 2.0-3.7 GPa[3-5] in human hair, 1.0-3.5 GPa[2] in porcupine quill, and 0.4 GPa[2,6] in hoof.

Due to the need in textile industry, intensive studies have examined this class of proteins from the 1930s onwards[7-11], aiming at understanding the explaining the mechanical behavior of keratin-based fibers and the link between the structural change and the mechanical properties. As a result of experimental work, several deformation models were proposed to interpret the shape of stress-strain curves, and to correlate with the fiber structure to explain the mechanical behavior of keratin fibers[12-21]. Earlier deformation mechanism models were proposed by Hearle[12-14] and Feughelman[15-19]. The deformation models used to describe the mechanical behavior of keratin fiber focus primarily on the geometric change of microfibril/matrix structure. In this earlier work the authors attempted to interpret the shape of curve in relation to the keratin IF protein (coiled coil structure) and an amorphous matrix structure. The major difference between these two models is that the Feughelman model does not take into account any interaction between the coiled coil region and matrix, while the model proposed by Chapman and Hearle incorporates a link between them. Besides these deformation models, previous computational studies of keratin proteins and other α-helical proteins, such as vimentin IF, focusing on the atomistic configuration and nanomechanical properties at atomistic scale have been reported[22-27]. However, relatively little is known of the basic physical material concepts that drive its deformation behavior, thus presenting an opportunity to generate a new approach that considers the structure-property paradigm from the atomistic level to the macroscopic scale. In order to provide a bottom-up description of materials behavior from a fundamental perspective, here we apply an atomistic multi-scale simulation approach that links the molecule's chemical structure (including the abundance of disulfide cross-links) and its larger-scale properties, and to upscale the molecular simulations based on the architecture of materials, especially to exploit insights that are relevant for bioengineering and other applications.

The study reported in this paper is aimed to build a mesoscopic simulation model of keratin macrofilaments and provide linking the micro-scale structural changes with the large-scale stress-strain curves of keratin fibers. We demonstrate that the deformation prediction from the mesoscopic model is in a good agreement with the stress-strain curve in experiments, and it provides insights and a general methodology to assess the mechanics of other biological systems.

Materials and Methods

Samples

Samples were randomly taken from a 39-year-old male donor and a 36-year-old female donor. Both pigmented (AC) and white (AW) male hairs belong to the same individual - age 39. Both pigmented (PC) and white (PW) female hairs belong to the same individual - age 36.

Tensile Testing Setup

The hair ends were cut off to isolate a central portion of about 60-70 mm. Then each sample edge was provided with a knot and subsequently glued to a cardboard support, resulting in a final net length as reported above. Testing apparatus is MTS Insight electrochemical testing system –1 kN – standard length. Tensile test is in displacement control. The load is applied up to specimen failure. The loading rate is 10 mm/min.

Mesoscale Modeling

In this study, a mesoscopic "bead-spring" method is used to investigate the mechanics of trichocyte keratin macrofilament with disulfide crosslinks. The method is a coarse-grained description of alpha-helical protein and matrix structure. It have proven to be a suitable approach to simulate certain aspects of alpha-helix based proteins, such as intermediate filaments in the cell's cytoskeleton[28,29] and other protein systems[30,31]. In the mesoscale model, each bead represents clusters of amino acids in explicit solvent, and all of beads interact according to a specific intermolecular multi-body potential to reflect the physical behavior of keratin proteins. The total

energy of the interaction of beads in the system, E_{tot}, is expressed as $E_{tot} = E_{bond} + E_{angle} + E_{non-bonded}$, (E1)

where E_{bond} is the bonded interaction describing the stretching behavior, E_{angle} is the bending energy, and $E_{non-bonded}$ is the nonbonded energy due to the van der Waals interactions. Within each intermediate filament, a multi-linear model is applied to model a nonlinear force-extension behavior of intermediate filament under stretching

$$\text{as} F(r) = -\frac{\partial E_{bond}(r)}{\partial r} = \begin{cases} k_1(r - r_0) & r < r_1 \\ k_1(r_1 - r_0) + k_2(r - r_1) & r_1 < r < r_2 \\ k_1(r_1 - r_0) + k_2(r_2 - r_1) + k_3(r - r_2) & r_2 < r < r_3 \\ k_1(r_1 - r_0) + k_2(r_2 - r_1) + k_3(r_3 - r_2) + k_4(r - r_4) & r_3 < r < r_4 \\ 0, & r_4 < r \end{cases} \quad \text{(E2)}$$

where $F(r)$ is the force between two beads, and k_1, k_2, k_3, k_4 are four spring constants which represent the stiffness of molecular stretching at different regimes as shown in Figure 2(A). The force-strain relationship in eq. (2) is fitted to reproduce the nanomechanical behavior obtained using the full atomistic model of keratin tetramer model[25] which has been well validated against experimental measurements. $E_{angle} = \frac{1}{2}k_\theta(\theta - \theta_0)^2$ with $k_\theta = \frac{3EI}{r_0}$, where EI is the bending stiffness, and θ is the angle between three beads relative to the equilibrium angle, θ_0. The bending stiffness, EI, can be obtained through the relationship of $EI = L_p k_B T$, where L_p is the intermediate filament persistence length, k_B is the Boltzmann constant and T is the temperature. The bending stiffness, EI, is obtained from bending deformation calculations of alpha-helical molecules in the previous publications[32,33]. The nonbonded interaction, $E_{non-bonded}$, is described by Lennard–Jones potential to simulate the van der Waals interactions between the filament chains and matrix-filament, $\phi_{LJ} = 4\varepsilon\left[\left(\frac{\sigma}{r}\right)^{12} - \left(\frac{\sigma}{r}\right)^{6}\right]$, where ε is the energy at equilibrium and σ is the distance as $\phi_{LJ} = 0$. A harmonic/shift/cut function in LAMMPS[34] with spring stiffness of 7.35 kcal/mol/Å^2 is applied to model the disulfide crosslinking. When the bond deformation is larger than 4 Å, the disulfide crosslinking breaks and the force drops to zero. The parameters are based on the full atomistic simulation results using ReaxFF reactive force field[35]. The time step used in our coarse-grained model is 20 fs. The simulations are performed using the large-scale atomic/molecular massively parallel simulator (LAMMPS)[34]. The mesoscopic parameters of the coarse-grained trichocyte keratin macrofilament model are summarized in Table 1.

In the coarse-grained model, the full length sequence of tetramer is replaced by a chains of beads, and eight chains of tetramer model is placed as a cylinder with diameter 7.0 nm to form an microfilament according the measurement using X-ray scattering on human hair[36,37]. The filaments are placed on a hexagonal lattice packing based on the observation in experiments shown in Figure 2(B). The distance between the center of mass of one filament and its nearest neighbor is determined by the experimental mean filament-filament distance 9.0 nm[36,37]. Assuming the eight chains are close packed on the cylinder, the diameter of one filament particle is roughly equal to the one-eighth of the circumference of the cylinder. Since a keratin tetramer is ~50 nm long and has a molecular weight of 200 kg/mol (around 2000 amino acids), one filament bead represents about 60 amino acids with a molecular weight of 12 kg/mol. The diameter of the matrix is determined using the separation between two filaments in order to place at least one particle between the filaments. For simplicity, assuming the density of the beads in our system is the same, we obtain that the molecular weight of the matrix bead is 4 kg/mol. Based on all of the structural parameters and the molecular weight fraction of microfibrils (43 %) and matrix (28 %) in experiments[38], we calculate the ratio of the number of filament and matrix beads equal to 12. Finally, the coarse-grained model containing the microfilaments embedded in the matrix is shown in Figure 2(C).

Mechanical Analysis in the Simulation

Pulling is applied in fiber-direction to model a tensile loading, as indicated in Figure 1(B). We stretch the systems by deform simulation box length in fiber-direction. In this study, we choose a small strain rate of 0.01 m/s which is computationally feasible, and no major rate effect on the system is observed. The simulations is carried out at 300 K in a NVT ensemble (constant temperature, constant volume, and constant number of particles). During the simulation, the pressure in fiber-direction and the box length are monitored to measure the stress-strain curve. The strain is defined by $\varepsilon = \Delta L/L$ (= engineering strain), where ΔL is the applied deformation and L is the length of the system in the pulling direction. Initial elastic modulus (Young's modulus) is calculated as the steepest slope of the stress-strain curve in the initial linear region.

Entropic hyperelasticity of helix

Hyperelasticity

Here, we use an entropic hyper-elasticity of helix model to describe the behaviour of alpha-helix domain in hair. The coil geometry shown in Figure 1(C) is described by the following equations:

$$x = r\cos 2\pi\frac{s}{l} \quad \text{(E3)}$$

$$y = r\sin 2\pi\frac{s}{l} \quad \text{(E4)}$$

$$z = \lambda\frac{s}{l} \quad \text{(E5)}$$

where r is the radius of the coil, s is the curvilinear coordinate, l is the length of a ring and λ is the distance between two adjacent rings. The coil angle is defined by $\tan\alpha = \frac{\lambda}{2\pi r}$.

If two self-equilibrated forces F are applied along z at the ends of the coil, its elastic energy per unit length will be:

$$\frac{dE_L}{ds} = \frac{1}{2}\left(\frac{N^2}{EA} + \frac{M^2}{GI_p}\right) \quad \text{(E6)}$$

where N is the axial load, M is the twisting moment, E and G are the material Young and shear modulus, A is the cross-section area and I_p is the torsional (e.g. polar, for circular cross- sections) moment of inertia of the fiber. It is worth noting that $M = Fr$, $N = F\sin\alpha$, we can easily derive the elastic energy in the coil composed by m rings, as:

$$E_L = \frac{m}{2}\frac{F^2}{EA}\left(\sin^2\alpha + 2(1+\nu)\frac{Ar^2}{I_p}\right)l \quad \text{(E7)}$$

where ν is the Poisson's ratio. The equivalent (in term of stored energy) elastic stiffness can be derived by comparison with:

$$E_L = \frac{1}{2}\frac{F^2}{K_E} \quad \text{(E8)}$$

yielding

$$K_E = \frac{EA/ml}{\sin^2\alpha + 2(1+\nu)\frac{Ar^2}{I_p}} \quad \text{(E9)}$$

Note that $\frac{Ar^2}{I_p}$ describes the slenderness of a ring and EA/l its axial stiffness.

Now we consider the actual values of r and α as imposed by a nominal strain $\varepsilon = \frac{\lambda-\lambda_0}{\lambda_0}$, where subscript 0 refers to the unstrained initial configuration. The strained coil geometry, described by the two functions $\alpha(\varepsilon)$ and $r(\varepsilon)$, can be deduced imposing the inextensibility of the coil (i.e.

neglecting the axial compliance with respect to the torsional one), i.e. imposing $l = l_0$, from which we obtain:

$$\sin\alpha(\varepsilon) = \sin\alpha_0\,(1+\varepsilon) \quad \text{(E10)}$$

then consequently

$$r(\varepsilon) = r_0\frac{\cos\alpha(\varepsilon)}{\cos\alpha_0} = r_0\sqrt{1-\frac{\varepsilon^2+2\varepsilon}{\frac{1}{\sin^2\alpha_0}-1}} \quad \text{(E11)}$$

The coil will reach the straight configuration ($\sin\alpha(\varepsilon^*) = 1$) under a critical strain:

$$\varepsilon^* = \frac{l-\lambda_0}{\lambda_0} = \frac{1}{\sin\alpha_0} - 1 \quad \text{(E12)}$$

Thus, in general, the hyper-elastic stiffness of a coil of contour length ml per cross-section area can be described by:

$$K_{HE}(\varepsilon) = K_E A\lambda_0 = \begin{cases} \dfrac{E\lambda_0/ml}{\sin^2\alpha_0(1+\varepsilon)^2 + 2(1+\nu)\frac{A}{I_p}r_0^2\left(1-\frac{\varepsilon^2+2\varepsilon}{\frac{1}{\sin^2\alpha_0}-1}\right)}, & \varepsilon < \varepsilon^* \\ \dfrac{E\lambda_0}{ml}, & \varepsilon \geq \varepsilon^* \end{cases} \quad \text{(E13)}$$

Hydrogen bonds (H-bonds)

We describe a stiffness of a linear elastic spring with a bundle of H-bonds between two adjacent coils as K_{HB}. We estimate the value of K_{HB} from the MD simulation results[39,40], where the 3.6 H-bonds in one convolution break simultaneously and the corresponding energy of H-bonds, and the corresponding energy barrier and the distance between the equilibrated state and the transition state are $E_{HB} = 11.1$ kcal/mol and $\Delta b_{HB} = 1.2$ Å. Thus K_{HB} can be obtained by

$$K_{HB} = \frac{(E_{HB}/\Delta b_{HB})N}{A} \quad \text{(E14)}$$

where N is the number alpha-helices in an unit area A. We apply the cross-section area ~10 nm^2 [41]of a tetramer that consists of 4 alpha-helices, and we obtain $K_{HB} = 254.8$ MPa.

Results and Discussion

In this study, we consider three different approaches to identify how the trichocyte keratin fiber with disulfide crosslink responds to mechanical deformation. First, tensile tests of hair samples in experiments. Second, a mesoscopic model of keratin macrofilament with disulfide crosslink. Finally, a we report a force-displacement relationship based on the helix-like theoretical model.

A series of tensile tests are performed to all the different hair samples. The results of stress-strain curves are shown in the **Figure 3**. Mean values of failure stress, failure strain, Young's modulus and toughness for the different hair samples are depicted in **Figure 4**. The results clearly show that the stress-strain curves of keratin fibers share a high level of similarity, and that there is almost no significant difference in the mechanical properties between different hair samples. The stress-strain curve of keratin fibers features the characteristic shape as shown in **Figure 3**, which can be divided into three different regimes based on the profile of the curve and varied physical phenomena related to each regime. The results are similar to the ones reported in literature. In the first regime, from 0 to ~4 % strain, the stress increases linearly with strain as an elastic behavior. In the second regime, from 4 to ~20 % strain, the stress reaches a plateau regime where the stress remains almost constant. It is found that unfolding of alpha-helical domains and a transition of alpha-helical to beta-sheet structure occur in this regime. In the last regime (strain > 20 %), the stress increases

again as the strain increases. The increased stiffness is caused by the stretching of covalent bonds of the protein backbone.

In order to further understand how the trichocyte keratin materials response under an external force, it is important to develop a model which reflects the composite structure of keratin materials and allows us to probe the effect of disulfide crosslinks. Since the experiments suggests that macrofilament serves the major component of trichocyte keratin[38], we build a mesoscopic model of the macrofilament consisting of microfilaments and matrix with disulfide crosslinks inside the matrix and in between the matrix and the microfilament as shown in **Figure 2**(C, D). Details about the model formulation are included in the ‘‘Materials and Methods’’ section.

We proceed with stretching the systems by deform simulation box length in fiber-direction and measure the stress-strain response of this material, until failure occurs. **Figure 5(A)** depicts stress-strain curves of the mesoscopic macrofilament model. We observe three major regimes in the stress-strain response. In the first regime (I), the stress increases linearly under a small deformation (strain < 7%). In the second regime (II), a relative flat increase in stress from 7 to 17 % strain, followed by an increasing stiffness of the stress, which lasts up to the stress close to 80 MPa (III). Eventually, strong bonds in the microfilaments chains break, and the entire system fails at 30 % strain. The phenomenon of the increase of the stress in the regime (III) is referred to as strain hardening.

The stress-strain curves of the mesoscopic simulation features the similar characteristic shape as the experimental measurements. From the analysis of the stress-strain behavior, the Young’s modulus = 1.38 GPa is calculated as the steepest slope of the stress-strain curve in the region (I). This modulus is close to experimental results for human hair, where a range of 1.1[42] to 6 GPa (our experiments) was reported. The maximum strain is for the mesoscpic filament model is predicted to be 30% (Fig. 5A) which is close to experimental measurements of ~33 %. We note that the maximum stress, 80MPa, of our mesoscopic model is almost twice smaller than the experimental data. The discrepancies between the experiments and the simulation might be caused by the fact that whole hair samples are considered in experiment, whereas a part of macrofilament system without any structural flaws is modeled in our simulations.

We further analyze the disulfide crosslink responses during the pulling. **Figure 5(B)** depicts the decrease of disulfide crosslink content which is normalized by the number of disulfide bond in the initial model plotted as a function of increasing applied strain. This plot also exhibits three different regimes during mechanical strain. The rupture of disulfide bonds occurs from the start of straining (0 to 7%). This shows the existence of the rupture of the linkages between the matrix and the IFs, and the result further supports Chapman and Hearle’s model that incorporates a link between the matrix and the IFs. In the second regime, the curve shows a small decrease in the crosslink content until ~17% strain, followed by a rapid decrease again until the system fractures. This phenomenon is consistent to the experimental measurement using Raman spectra[43]. **Figure 5(C)** shows the simulation snapshots of the macrofilament at different applied strains. Under strain, the microfilaments deform cooperatively, and the chains start aligning along the fiber direction. At the larger strain, once a bundle of the microfilaments breaks, then the system fails. Despite its simplicity, our model captures the essential physical properties of alpha-helical based keratin macrofilaments as identified in earlier theoretical and experimental studies. Through simulation of a larger-scale filament and matrix structure, our model enables us to provide an important link between single molecule properties and mechanisms and the overall material behavior at much larger length-scales.

We proceed with the study of mathematical equation of hyper-elastic stiffness coil model linking the structural change and stress-strain curve of keratin fiber through a spring model. Under small

deformation, the stretch of H-bonds in convolutions of alpha-helical structure in keratin proteins plays the major role. The stiffness of an alpha-helix can be calculated as (H-bonds in parallel to the elasticity of a coil plotted in **Figure 6(A)**)

$$K = K_{HB} + K_{HE} \quad \text{(E15)}$$

Once the deformation of H-bonds elongates to a critical points Δb_{HB} which is the critical displacement for H-bond fracture, the unfolding of alpha-helix occurs. We consider a chain with N units of folded structure involved in H-bond fracture and assume the ratio of units of folded structure is $\frac{Nx_\alpha}{L\,(N)} = \frac{Nx_\alpha}{(L_0+Nx_\alpha)} = 0.15$, where $L\,(N)$ is the total length of the chain, L_0 is the length of chains not involved in H-bond fracture and x_α is the unit length of helix. Thus due to $\frac{\Delta b_{HB}}{x_\alpha} = \frac{1.2}{5.4} = 0.22$, the critical strain for the rupture of H-bonds $\varepsilon_1 = \frac{N\Delta b_{HB}}{(L_0+Nx_\alpha)} = 0.03$ can be obtained. Beyond the critical point ε_1, the helical structures start to unfold, and the regime is dominated by the hyper-elasticity mechanics until the coil reaches the straight configuration where the backbone of the protein starts to be stretched at the strain ε^* in (E13). It is known that the ratio of the unit length of helix (x_α) to its contour length (λ) is about 0.5, i.e. $\varepsilon^* = \frac{\lambda - x_\alpha}{x_\alpha} \approx 1.0$; based on the previous atomistic simulation[22], assuming the ratio of the length of helix structure (Mx_α) involved in the unfolding $\frac{Mx_\alpha}{L\,(N)} = \frac{Mx_\alpha}{(L_1+Mx_\alpha)} \approx 0.4$, where L_1 is the length of chains not involved in unfolding, thus the critical strain for the alpha-helix unfolding is $\varepsilon_2 = \frac{M(\lambda - x_\alpha)}{(L_1+Mx_\alpha)} = 0.4$. After the hyper-elasticity regime where $\varepsilon < \varepsilon_2$, the intrinsic axial stiffness of the fiber, $K_{HE} = \frac{E\lambda_0}{ml}$, dominates up to fracture.

Here we further apply a binomial distribution to consider the effect of disulphide crosslinks in the system. We assume that the number of breaking disulfide bonds is k, each with a bond breaking probability p. The total number of disulfide bond is n so that the probability of k bonds breaking in a pulling event is given by a binomial distribution:

$$b = \binom{n}{k} p^k (1-p)^{n-k} . \quad \text{(E16)}$$

Moreover, we assume that after certain amount x of disulfide bond are broken, the system fails, so that the probability that the total number X of disulfide bond breaking during the entire pulling process with a given probability distribution b will exceed the tolerance x is given by

$$B = 1 - \sum_{i=0}^{\mathrm{x}} \binom{n}{i} p^i (1-p)^{n-i} . \quad \text{(E17)}$$

The parameters used in the binomial distribution are obtained by fitting the failure stress, failure strain and the critical point at the onset of the third regime in stress-strain curves of keratin fibers. Thus, considering the breaking of disulfide bond under stretching, the stiffness of an alpha-helical chain of can be described by

$$K = B(K_{HE} + K_{HB}) \quad \text{(E18)}$$

Based on the stiffness in Equation (19), the stress-strain relationship is given by $\sigma = K\varepsilon$, where σ is the stress and ε is the engineering strain. **Figure 6(B)** depicts the stress-strain curve of the alpha-helical chain, and the result agrees quite well with the experimental data. We also compare the mesoscale simulation results with experimental data and theoretical prediction plotted in **Figure 6(C)**. The stress and strain are normalized to the maximum values in each data set, individually, to compare the shape of stress-strain curves and the mechanical response in tensile testing. The comparison in **Figure 6(C)** shows that the stress-strain curves have similar shape which features three regimes. In the first regime (I), both stresses increase linearly with strain. In the second (II), a stress plateau relates to the unfolding of the coiled-coil segments and alpha-helical structure. For the third (III) regime, the stretching of the backbone of the alpha-helix with the breaking of disulfide crosslinks causes the strain stiffening of the material, and the system fails.

Conclusion

The study reported here presented a mesoscopic coarse-grained model to link the microscopic structure of trichocyte keratin fibers to the mechanical properties at larger scales. The composite structure of keratin fiber at the mesoscale is addressed using a bead-spring model for a keratin macrofilament. Mesoscale beads represent coil-coiled keratin tretramer proteins which are assembled to filaments and embedded in a matrix of soft particles with disulfide crosslinks. The mesoscopic model gives good agreement with a wide range of experimental results. The stress-strain curve of hair fibers predicted by the mesoscopic model agrees well with our experimental data. The disulfide crosslink the microfibril-matrix and matrix-matrix contributes the initial modulus and provides stiffening at larger deformation of trichocyte keratins. The results show that the disulfide bonds reinforce the macrofilament and enhance the robustness of the macrofilament by facilitating the microfilaments to deform cooperatively. The availability of the coarse-grained multi-scale model now allows us to study the mechanical properties at larger scales of keratin fibrils, and perhaps entire hair fibers. The mesoscopic model of keratin fiber built here could be directly extended to other soft fibrous-matrix materials, such as porcupine quills.

Notes and acknowledgements: C.C.C. and M.J.B. acknowledge funding from AFOSR whereas N.M.P. from the European Research Council (ERC), the European Union's (EU), and the Provincia Autonoma di Trento (PAT), respectively: ERC StG 2011 “Bihsnam”, ERC PoC 2013 “Replica^{2}”, ERC PoC 2013 “Knotough”, EU Graphene Flagship “Nanocomposites” and PAT “Graphene Nanocomposites”.

References

(1) Oxenham, W. *British Polymer Journal* **1989**, *21*, 279.

(2) Chou, S. F.; Overfelt, R. A. *Mat Sci Eng C-Mater* **2011**, *31*, 1729.

(3) Seshadri, I. P.; Bhushan, B. *Acta Materialia* **2008**, *56*, 774.

(4) Fudge, D. S.; Gosline, J. M. *Proceedings of the Royal Society of London. Series B: Biological Sciences* **2004**, *271*, 291.

(5) Guthold, M.; Liu, W.; Sparks, E.; Jawerth, L.; Peng, L.; Falvo, M.; Superfine, R.; Hantgan, R.; Lord, S. *Cell Biochemistry and Biophysics* **2007**, *49*, 165.

(6) Bertram, J. E.; Gosline, J. M. *Journal of Experimental Biology* **1987**, *130*, 121.

(7) Speakman, J. B. *Journal of the Textile Institute Transactions* **1927**, *18*, T431.

(8) Astbury, W. T.; Woods, H. J. *Philos. Trans. R. Soc. Lond. A-Contain. Pap. Math. Phys. Character* **1934**, *232*, 333.

(9) Astbury, W. T.; Street, A. *Philos. Trans. R. Soc. Lond. A-Contain. Pap. Math. Phys. Character* **1932**, *230*, 75.

(10) Kreplak, L.; Doucet, J.; Briki, F. *Biopolymers* **2001**, *58*, 526.

(11) Kreplak, L.; Doucet, J.; Dumas, P.; Briki, F. *Biophysical Journal* **2004**, *87*, 640.

(12) Hearle, J. W. S. *Textile Research Journal* **1969**, *39*, 1109.

(13) Hearle, J. W. S. *International Journal of Biological Macromolecules* **2000**, *27*, 123.

(14) Hearle, J. W. S. *Journal of Polymer Science Part C: Polymer Symposia* **1967**, *20*, 215.

(15) Feughelman, M.; Haly, A. R. *Biochim Biophys Acta* **1959**, *32*, 596.

(16) Feughelman, M. *J Macromol Sci Phys* **1979**, *B16*, 155.

(17) Feughelman, M. *Textile Research Journal* **1994**, *64*, 236.

(18) Feughelman, M. *Mechanical Properties and Structure of Alpha-keratin Fibres: Wool, Human Hair and Related Fibres*; UNSW Press: Sydney, 1997.

(19) Feughelman, M. *Journal of Applied Polymer Science* **2002**, *83*, 489.

(20) Wortmann, F.-J.; Zahn, H. *Textile Research Journal* **1994**, *64*, 737.

(21) Chapman, B. M.; Feughelman, M. *Journal of Polymer Science Part C: Polymer Symposia* **1967**, *20*, 189.

(22) Qin, Z.; Kreplak, L.; Buehler, M. J. *Plos One* **2009**, *4*.

(23) Qin, Z.; Buehler, M. *Journal of Molecular Modeling* **2011**, *17*, 37.

(24) Qin, Z.; Chou, C.-C.; Kreplak, L.; Buehler, M. In *Advances in Cell Mechanics*; Li, S., Sun, B., Eds.; Springer Berlin Heidelberg: 2012, p 117.

(25) Chou, C. C.; Buehler, M. J. *Biomacromolecules* **2012**, *13*, 3522.

(26) Azoia, N. G.; Fernandes, M. M.; Micaêlo, N. M.; Soares, C. M.; Cavaco-Paulo, A. *Proteins: Structure, Function, and Bioinformatics* **2012**, *80*, 1409.

(27) Akkermans, R. L. C.; Warren, P. B. *Philosophical Transactions of the Royal Society of London. Series A: Mathematical, Physical and Engineering Sciences* **2004**, *362*, 1783.

(28) Ackbarow, T.; Sen, D.; Thaulow, C.; Buehler, M. J. *Plos One* **2009**, *4*.

(29) Qin, Z.; Buehler, M. J. *Theoretical and Applied Mechanics Letters* **2012**, *2*.

(30) Buehler, M. J. *Proceedings of the National Academy of Sciences* **2006**, *103*, 12285.

(31) Buehler, M. J. *Nanotechnology* **2007**, *18*.

(32) Ackbarow, T.; Buehler, M. *Journal of Materials Science* **2007**, *42*, 8771.

(33) Buehler, M. J. *J Mech Mater Struct* **2007**, *2*, 1019.

(34) Plimpton, S. *Journal of Computational Physics* **1995**, *117*, 1.

(35) Keten, S.; Chou, C. C.; van Duin, A. C. T.; Buehler, M. J. *Journal of the Mechanical Behavior of Biomedical Materials* **2012**, *5*, 32.

(36) Kreplak, L.; Franbourg, A.; Briki, F.; Leroy, F.; Dallé, D.; Doucet, J. *Biophysical Journal* **2002**, *82*, 2265.

(37) Kajiura, Y.; Watanabe, S.; Itou, T.; Nakamura, K.; Iida, A.; Inoue, K.; Yagi, N.; Shinohara, Y.; Amemiya, Y. *Journal of Structural Biology* **2006**, *155*, 438.

(38) Zahn, H. *International journal of cosmetic science* **2002**, *24*, 163.

(39) Ackbarow, T.; Buehler, M. J. *J. Comput. Theor. Nanosci.* **2008**, *5*, 1193.

(40) Ackbarow, T.; Keten, S.; Buehler, M. J. *J Phys-Condens Mat* **2009**, *21*.

(41) Sokolova, A. V.; Kreplak, L.; Wedig, T.; Mücke, N.; Svergun, D. I.; Herrmann, H.; Aebi, U.; Strelkov, S. V. *Proceedings of the National Academy of Sciences* **2006**, *103*, 16206.

(42) Greenberg, D. A.; Fudge, D. S. *Proceedings of the Royal Society B: Biological Sciences* **2013**, *280*.
(43) Paquin, R.; Colomban, P. *J Raman Spectrosc* **2007**, *38*, 504.

Tables and Table Legends

Table 1. Summary of the parameters used in the mesoscopic model

Parameter and units	Numerical value
Equilibrium bead distance r_0 (Å)	28
Critical distances r_1, r_2, r_3, r_4 (Å)	30.257, 45.96, 57.93, 75.6
Tensile stiffness parameters k_1, k_2, k_3, k_4 (kcal/mol/Å^2)	4.49, 0.0, 0.46, -0.86
Equilibrium angle θ_0 (º)	180
Bending stiffness parameter k_θ (kcal/mol/rad^2)	3.44
Equilibrium energy ε (kcal/mol)	6.8
Equilibrium distance σ (Å)	25

Table 2. Overview of experimental specimens

	AC series	AW series	PC series	PW series
Specimen description	Pigmented male hair (°)	White male hair (°)	Pigmented female hair (§)	White female hair (§)
Number of specimens	10	10	10	10
Diameter (#) (μm)	68.60	71.82	61.55	78.08
Length (*) (mm)	AC01 39.1 AC02 38.2 AC03 43.2 AC04 37.2 AC05 41.9 AC06 44.4 AC07 46.2 AC08 33.6 AC09 45.6 AC10 36.2			
	AW01 33.6 AW02 34.5 AW03 42.5 AW04 34.7 AW05 34.3 AW06 42.2 AW07 35.7 AW08 45.1 AW09 31.8 AW10 35.9			
	PC01 40.0 PC02 48.3 PC03 36.8 PC04 38.8 PC05 45.2 PC06 32.5 PC07 46.4 PC08 44.1 PC09 43.2 PC10 43.5			
	PW01 32.3 PW02 32.1 PW03 30.1 PW04 31.8 PW05 30.9 PW06 33.9 PW07 31.7 PW08 38.8 PW09 33.1 PW10 34.4			
Notes	(°) Both pigmented and white male hairs belong to the same individual - age 39. (§) Both pigmented and white female hairs belong to the same individual - age 36. (#) Mean value over 18 measurements, performed on 3 hairs per series, using SEM. (*) The specified values refer to net lengths, after sample preparation for test.			

Figures and Figure Captions

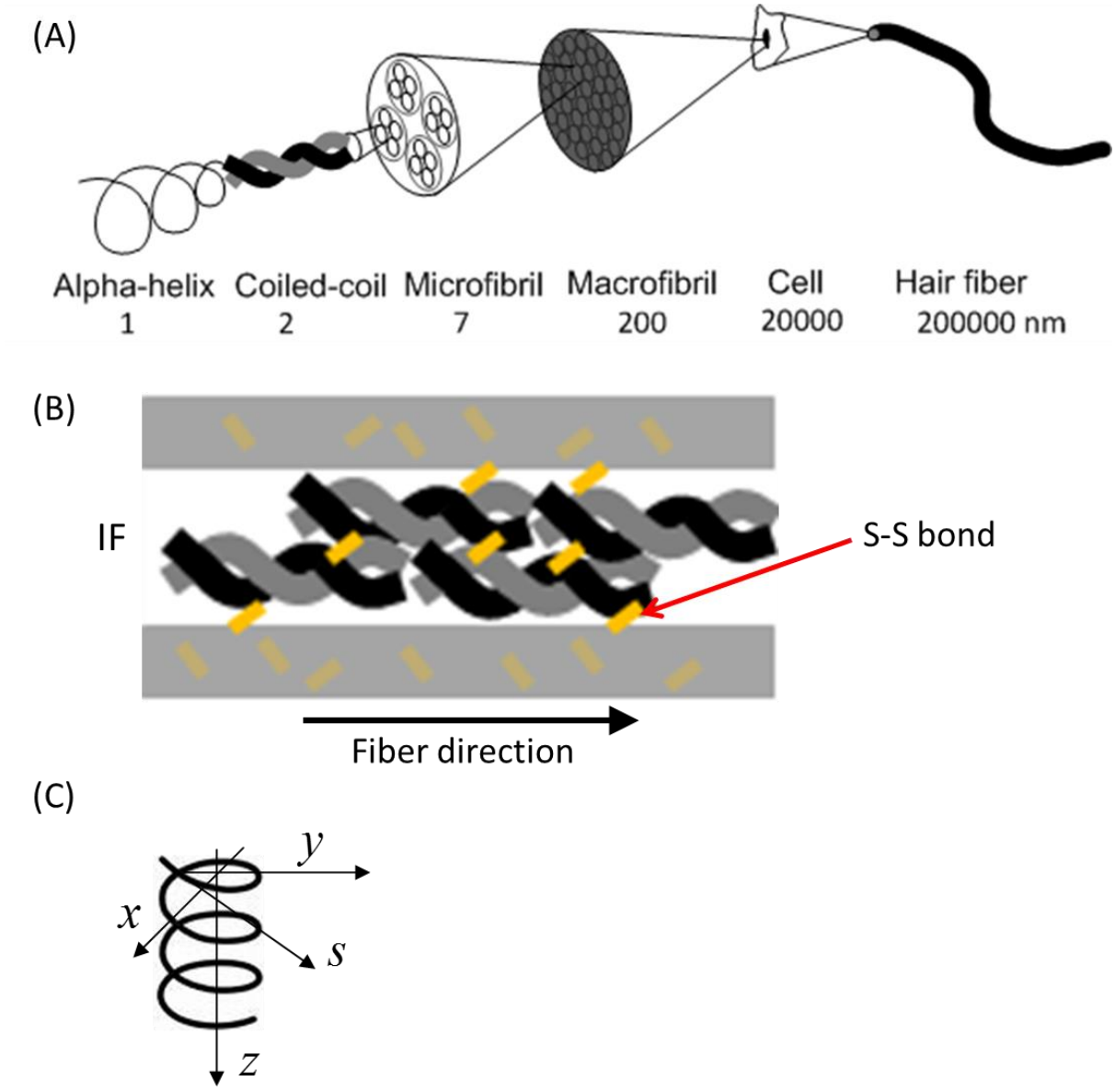

FIGURE 1. (A) Human hair features a hierarchical structure, ranging from alpha-helix, dimers with a coiled-coil structure, microfibrils, macrofibrils to the cellular and eventually entire hair fiber level. (B) Schematic visualization that shows IFs are embedded in the matrix connected by intramolecular disulfide bonds (S-S bond in the figure). (C) Geometry of the coil and reference system.

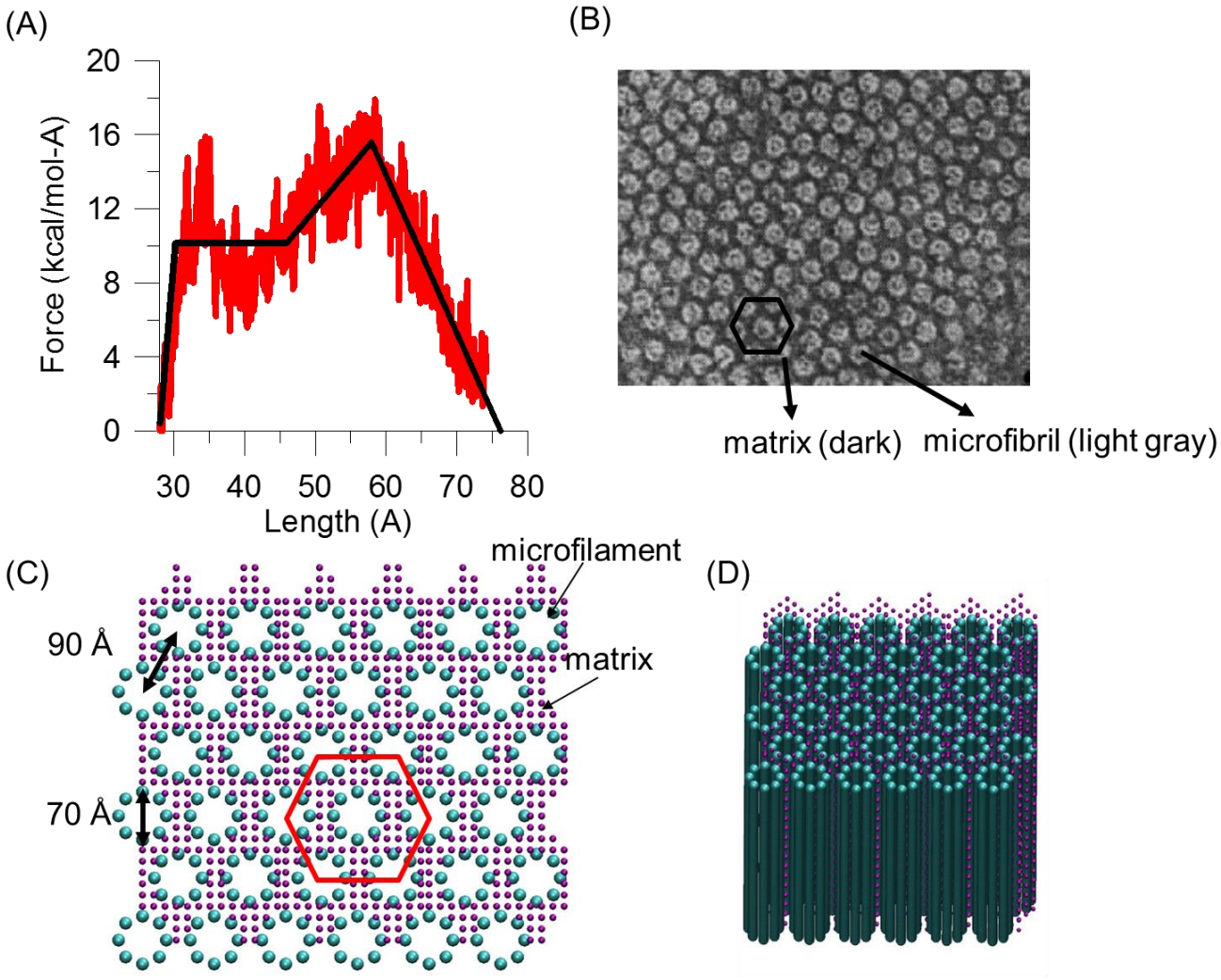

FIGURE 2. (A) The force-strain relationship of individual keratin microfilament in our bead-spring model is derived from full-atomistic simulations[25] and has been validated against experimental studies. (B) Electron micrograph of the central portion of macrofibril in the cortex of fine wool depicts the hexagonal microfibril packing in macrofibril. (C) Coarse-grained model of keratin macrofibril. The filaments are placed on a hexagonal lattice.

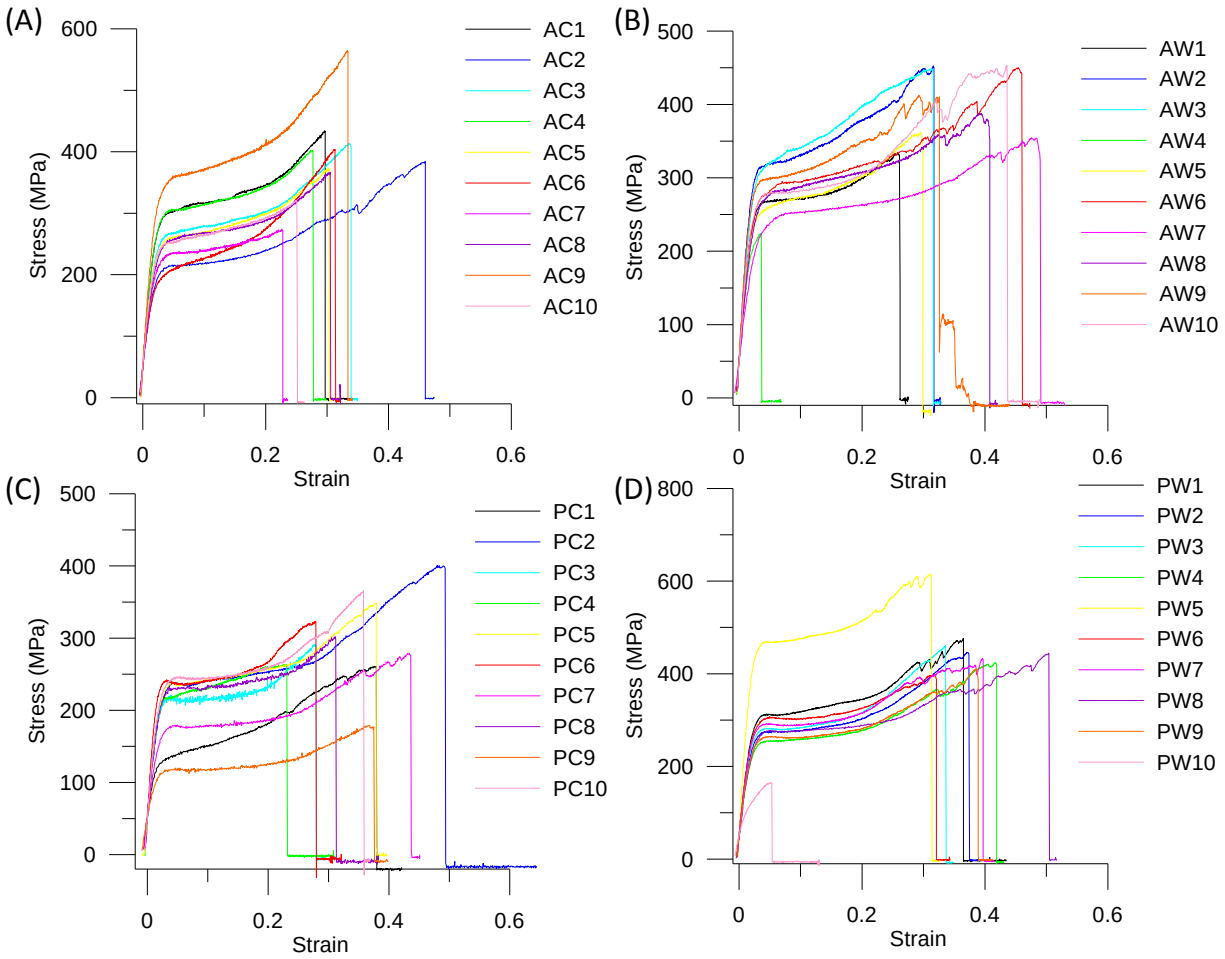

FIGURE 3. Tensile stress-strain curves of (A) pigmented male hair (AC), (B) white male hair (AW), (C) pigmented female hair (PC) and (D) white female hair (PW).

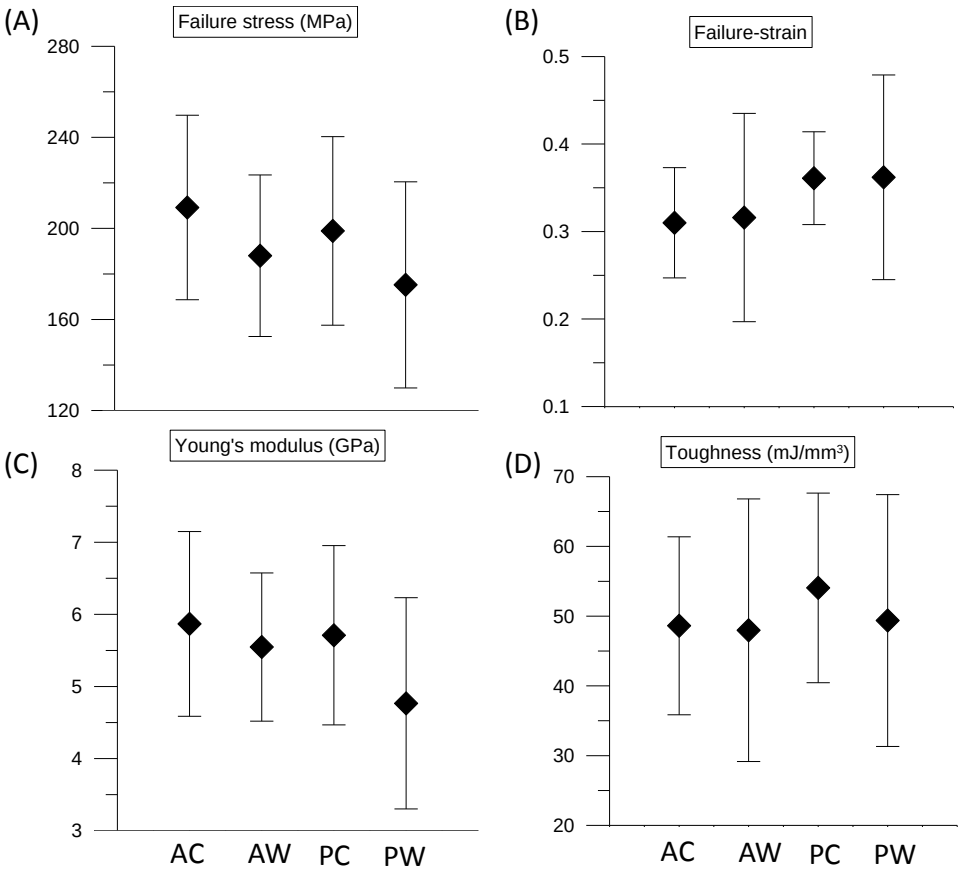

FIGURE 4. Mechanical properties of AC, AW, PC and PW under external tensile loading. (A) Failure stress, (B) Failure strain, (C) Young's modulus and (D) Toughness.

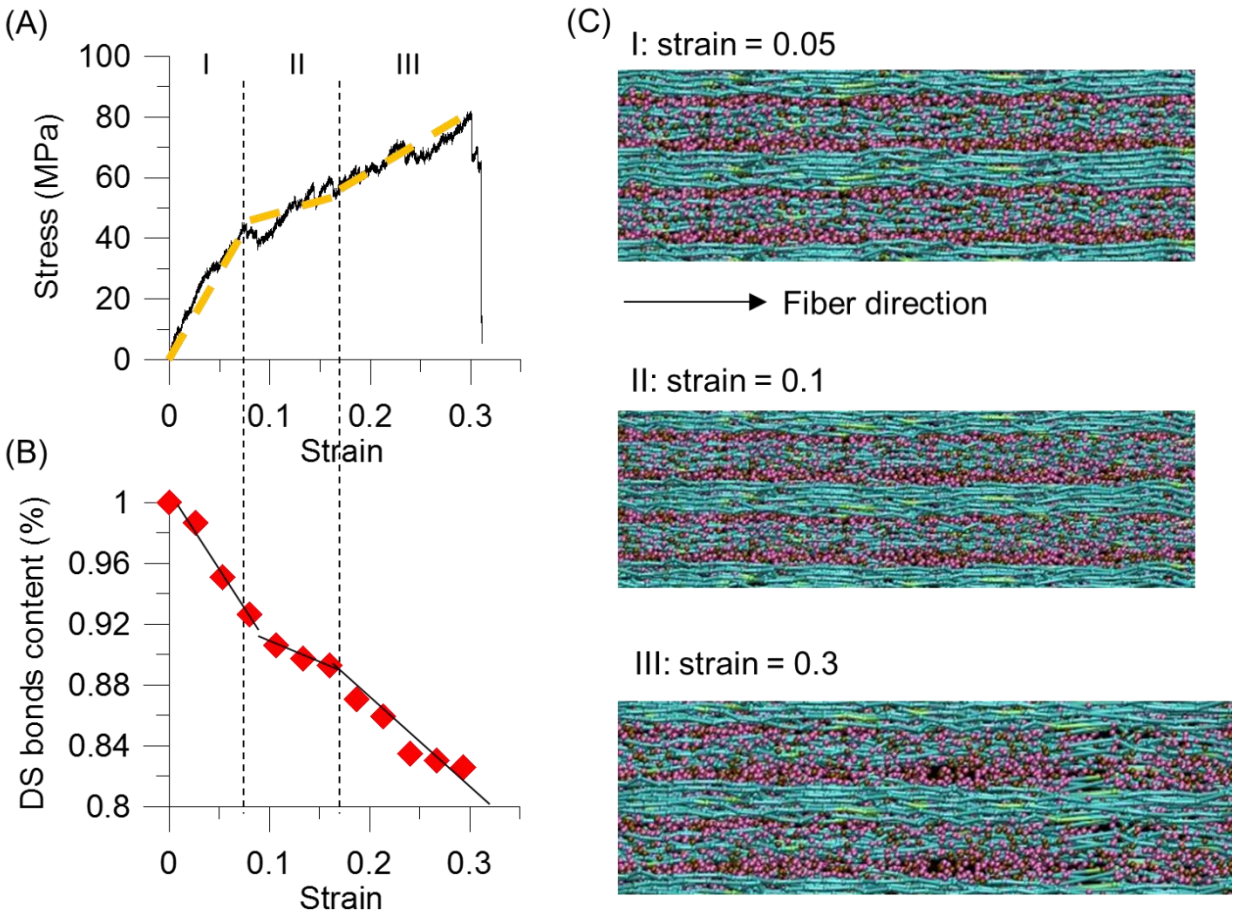

FIGURE 5. (A) The stress-strain curves of coarse-grained simulation. (B) Decrease of disulfide crosslink content, normalized by the number of disulfide bond in the initial model. (C) Simulation snapshots at different pulling strains.

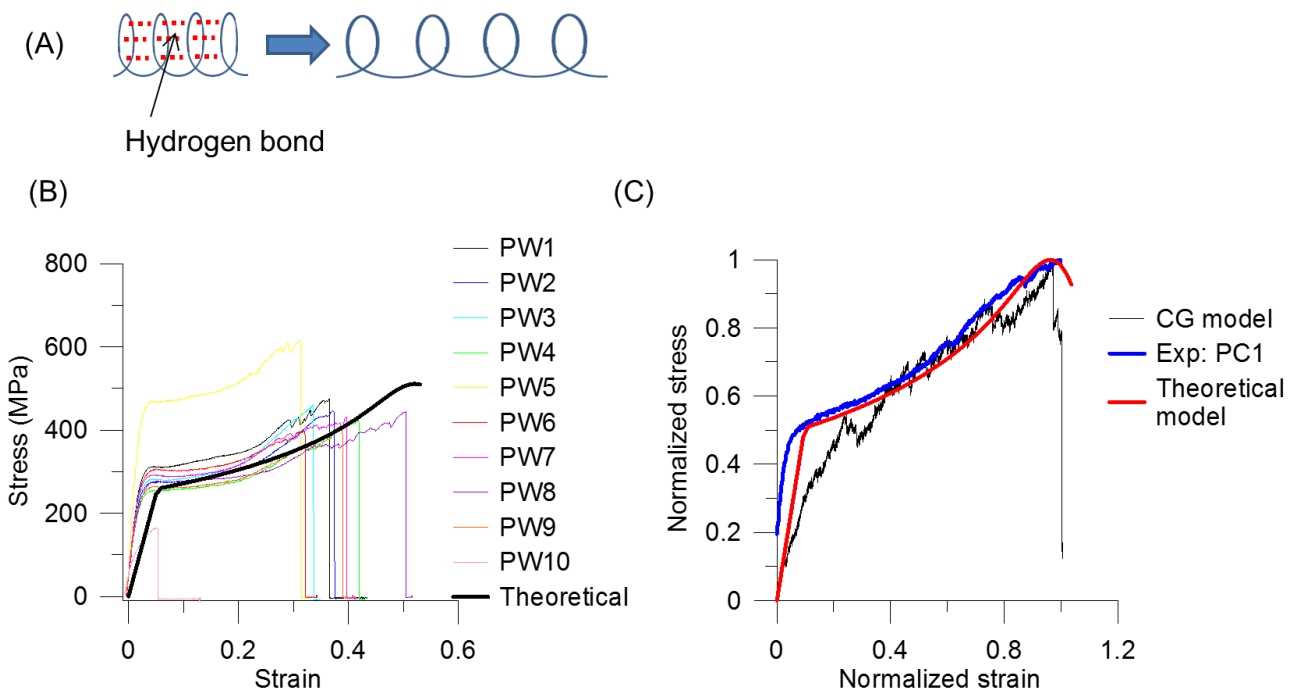

FIGURE 6. (A) Illustration of H-bonds in parallel in coils and unfolding of the helical structures (B) Comparison of stress-strain curves of experimental data and theoretical prediction based on the stiffness in Equation (E19), where the parameters in binomial distribution are obtained by fitting the failure stress, failure strain and the critical point at onset of third regime in stress-strain curves of keratin fibers. (C) Comparison of normalized stress-strain curves of coarse-grained simulation, theoretical prediction and experimental data. The stress and strain are normalized to the maximum values in each data set, individually, to compare the shape of stress-strain curves and the mechanical response in tensile testing.